CM^2 Magazine

第 141 期

南方科技大学海洋磁学中心主编

https://cm2.sustech.edu.cn/

创刊词

海洋是生命的摇篮，是文明的纽带。地球上最早的生命诞生于海洋，海洋里的生命最终进化成了人类，人类的文化融合又通过海洋得以实现。人因海而兴。

人类对海洋的探索从未停止。从远古时代美丽的神话传说，到麦哲伦的全球航行，再到现代对大洋的科学钻探计划，海洋逐渐从人类敬畏崇拜幻想的精神寄托演变成可以开发利用与科学研究的客观存在。其中，上个世纪与太空探索同步发展的大洋科学钻探计划将人类对海洋的认知推向了崭新的纬度：深海（deep sea）与深时（deep time）。大洋钻探计划让人类知道，奔流不息的大海之下，埋藏的却是亿万年的地球历史。它们记录了地球板块的运动，从而使板块构造学说得到证实；它们记录了地球环境的演变，从而让古海洋学方兴未艾。

在探索海洋的悠久历史中，从大航海时代的导航，到大洋钻探计划中不可或缺的磁性地层学，磁学发挥了不可替代的作用。这不是偶然，因为从微观到宏观，磁性是最基本的物理属性之一，可以说，万物皆有磁性。基于课题组的学科背景和对海洋的理解，我们对海洋的探索以磁学为主要手段，海洋磁学中心因此而生。

海洋磁学中心，简称 CM^2，一为其全名“Centre for Marine Magnetism”的缩写，另者恰与爱因斯坦著名的质能方程 $E = MC^2$ 对称，借以表达我们对科学巨匠的敬仰和对科学的不懈追求。

然而科学从来不是单打独斗的产物。我们以磁学为研究海洋的主攻利器，但绝不仅限于磁学。凡与磁学相关的领域均是我们关注的重点。为了跟踪反映国内外地球科学特别是与磁学有关的地球科学领域的最新研究进展，海洋磁学中心特地主办 CM^2 Magazine，以期与各位地球科学工作者相互交流学习、合作共进！

“海洋孕育了生命，联通了世界，促进了发展”。21 世纪是海洋科学的时代，由陆向海，让我们携手迈进中国海洋科学的黄金时代。

目 录

1. 轨道岁差调控下太平洋冷舌两个年周期旋回

翻译人：仲义 zhongy@sustech.edu.cn

Chiang, J.C.H., Atwood, A.R., Vimont, D.J., et al. ***Two annual cycles of the Pacific cold tongue under orbital precession*** *[J] Nature, 2022, 611(7935), 295-300.*

https://doi.org/10.1038/s41586-022-05240-9

摘要：太平洋冷舌海温的年周期被认为是由于地球的轴向倾斜驱动所影响，因此它的相位应该相对于日历时间所固定。然而，在多种地球系统模型当中，通过不同的轨道岁差调控，其相位和振幅发生显著和一致性的变化。本文，作者发现冷舌具有另外一个年代际周期旋回，受控于轨道偏心率引起的地球-太阳距离变化。因为这两个周期具有轻微不同的周期性，它们的扰动导致在一个岁差周期里面复杂的季节性演变。由于距离效应产生的振幅随着偏心率线性增加，与过去 100 万年中最大偏心率的倾斜效应振幅相当（值为 0.05）。从机制上讲，对冷舌的距离效应是通过沃克环流的季节性径向位移及年际风场强迫产生的热带太平洋海洋-大气动力系统。这一发现呼吁我们需要重新评估目前太平洋冷舍的理解和热带太平洋年周期相位变化。

ABSTRACT: The Pacific cold tongue annual cycle in sea surface temperature is presumed to be driven by Earth's axial tilt1–5 (tilt effect), and thus its phasing should be fixed relative to the calendar. However, its phase and amplitude change dramatically and consistently under various configurations of orbital precession in several Earth System models. Here, we show that the cold tongue possesses another annual cycle driven by the variation in Earth–Sun distance (distance effect) from orbital eccentricity. As the two cycles possess slightly different periodicities6, their interference results in a complex evolution of the net seasonality over a precession cycle. The amplitude from the distance effect increases linearly with eccentricity and is comparable to the amplitude from the tilt effect for the largest eccentricity values over the last million years (e value approximately 0.05) 7. Mechanistically, the distance effect on the cold tongue arises through a seasonal longitudinal shift in the Walker circulation and subsequent annual wind forcing on the tropical Pacific dynamic ocean–atmosphere system. The finding calls for reassessment of current

understanding of the Pacific cold tongue annual cycle and re-evaluation of tropical Pacific paleoclimate records for annual cycle phase changes.

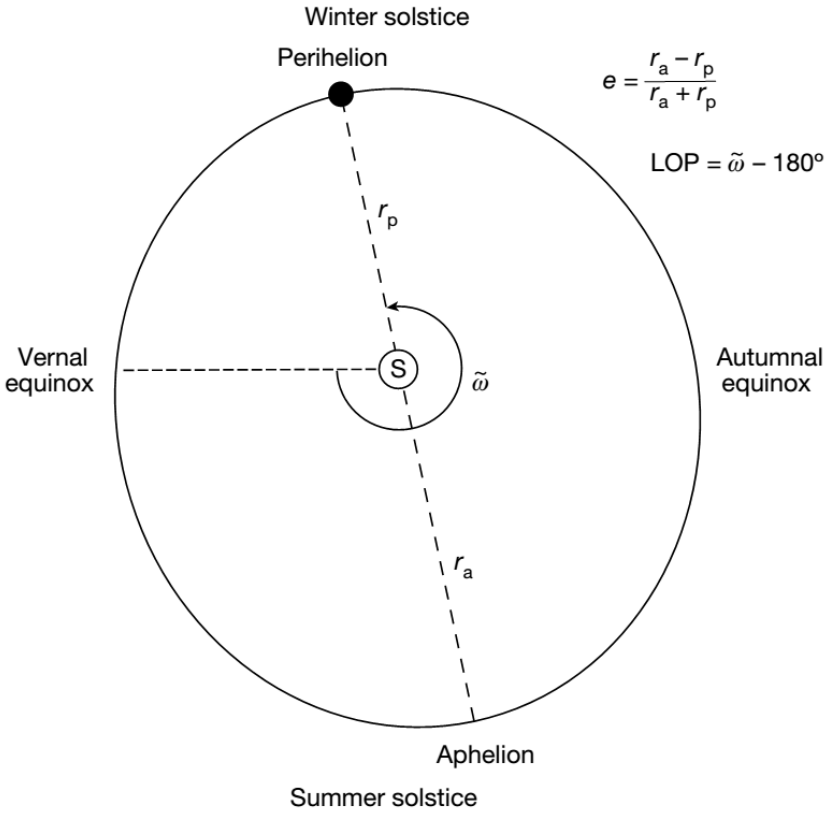

Figure 1. Schematic of the Earth's orbital configuration. The Earth's orbit around the Sun (marked S) is elliptical with the Sun at one focal point and with the closest approach at perihelion (at a distance rp) and furthest at aphelion (ra). The direction of the orbit is counterclockwise. The eccentricity e, defined in the figure, measures how elliptical the orbit is: e = 0.0493 is used for the simulations reported in Fig. 2, about three times larger than the modern-day value. The equinox and solstice points are named following Northern hemisphere seasons. The LOP relative to the moving vernal equinox is defined (following Fig. 8 of ref. 38) as the angular distance from vernal equinox to perihelion following Earth's orbit ($\tilde{\omega}$, in degrees), subtracted by 180°. Thus, LOP is 90° and 180° if perihelion occurs during winter solstice and vernal equinox, respectively. Perihelion, as drawn in the schematic, is positioned for modernday, with an LOP of about 103° and date of around 3 January. Because the distance effect annual cycle (from perihelion to perihelion, otherwise called the anomalistic year, 365.259636 d (ref. 6)) is slightly longer than the tilt effect annual cycle (from equinox to equinox, otherwise known as the tropical year, 365.242189 d (ref. 6)), the LOP increases over time. A complete revolution of the LOP is the precession cycle, about 22,000 yr (ref. 38). Note

that the Gregorian calendar is referenced to the vernal equinox, with its rule for leap days designed to resynchronize the calendar year with the tropical year.

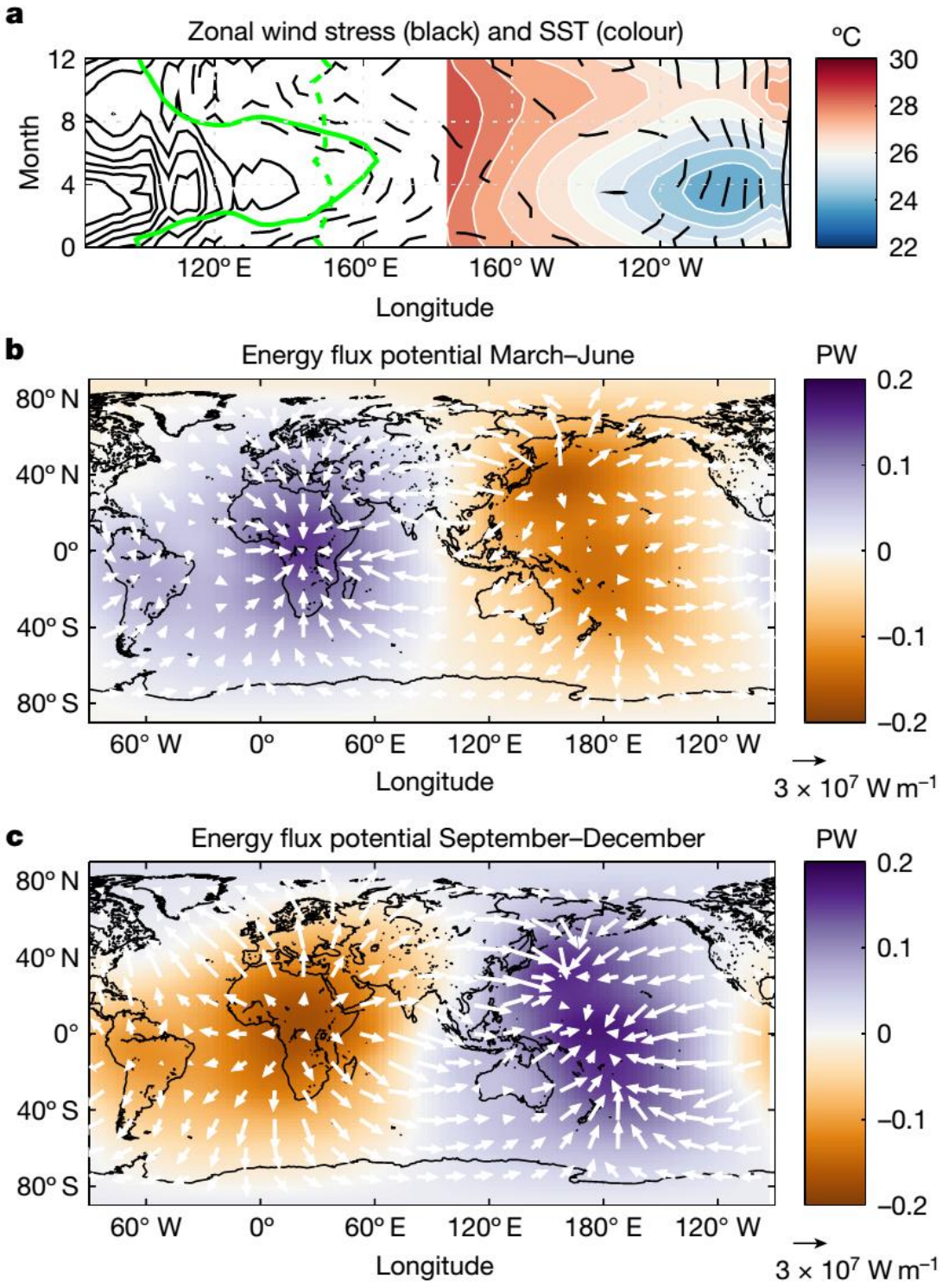

Figure 2. The distance effect on the longitude position of the Walker circulation as diagnosed by the energy flux potential. a, Equatorial Pacific zonal wind stress (black contours, contour interval

1×10^{-2} N m $^{-2}$; dashed contours are negative and zero contour not shown) and SST (shaded) averaged over 6° S–6° N for the distance-only run (obliquity = 0°, e = 0.05, LOP = 0°). Positive values of wind stress correspond to westerly winds. Because the focus is on the cold tongue, SST is only shown east of the date line; also, an offset is added so that the annual mean SST averaged over 145° E–85° W is the same as for the observational data, as shown in Extended Data Fig. 1a, 27.44 °C. The solid green line shows the EFPM over the western Pacific for the distance-only run and the dashed green line for the zero annual forcing run. b, Energy flux potential (shaded, units are petawatts (PW)) averaged over March–June, for the difference between the distance-only and zero annual forcing runs (the former minus the latter). The vectors correspond to the difference in the divergent horizontal atmospheric energy transport. c, Same as b but for September–December. See Methods section on 'Atmospheric energy flux analysis' for details on the calculations. The Map package 41 was used to generate the maps in b and c, using coastline data from the global self-consistent, hierarchical, high-resolution geography database.

2. 什么条件有助于非典型俯冲:来自 Mussau 海沟、Hjort 海沟和 Gagua 海脊的启示

翻译人：刘伟 inewway@163.com

Wang X, Gao L, Zhao M, et al. ***What conditions promote atypical subduction: Insights from the Mussau Trench, the Hjort Trench, and the Gagua Ridge****?[J].* ***Gondwana Research****, 2022.*

https://doi.org/10.1016/j.gr.2022.10.014

摘要：俯冲带是地壳和地幔之间物质交换的界面。西太平洋板块区域是在一个汇聚板块构造环境演化区域。老的大洋板块通常会在年轻的大洋板块之下俯冲，例如 IBM 和汤加-克马德克俯冲带。然而，在一些俯冲带，如 Mussau 海沟，Hjort 海沟和 Gagua 海脊，年轻和密度更小的海洋板块已经被确认俯冲在更老和密度更大的板块下面。是什么条件促进了非典型俯冲，仍然不清楚。本文以 Mussau 海沟、Hjort 海沟和 Gagua 海脊为例，探讨了控制非典型俯冲形成的潜在因素。通过对 Mussau 海沟和 Hjort 海沟构造特征的分析，发现板块边界以走滑主导式挤压为主时，非典型俯冲作用可能是可行的；也就是说，走滑成分超过挤压成分，这可能与 Gagua 海脊发生的非典型俯冲相反，至少目前是这样。结合 Mussau 海沟和 Hjort 海沟的演化，进一步认为俯冲极性反转和走滑边界是非典型俯冲的关键。

ABSTRACT: Subduction zones act as interfaces for exchanging materials between the Earth's crust and mantle. The western Pacific plate region is evolving within a convergent tectonic environment. Old oceanic plates generally subduct beneath young oceanic plates, as exemplified by the Izu-Bonin-Mariana and Tonga-Kermadec subduction zones. However, in some subduction zones, such as the Mussau Trench, the Hjort Trench, and the Gagua Ridge, young and more buoyant oceanic plates have been recognized to subduct underneath older and denser plates. What conditions promote atypical subduction, however, remain elusive. In this study we take the Mussau Trench, the Hjort Trench, and the Gagua Ridge as examples to explore the possible underlying factors that control the formation of atypical subduction. By anatomizing the tectonic features of both the Mussau Trench and the Hjort Trench, we find that atypical subduction may be feasible mainly when

the plate boundary is characterized by strike-slip-dominated transpression; that is, the strike-slip component overwhelms the compression component, which may argue against the atypical subduction occurring at the Gagua Ridge, at least at present. Moreover, in light of the evolution of both the Mussau Trench and the Hjort Trench, it is further suggested that subduction polarity reversal and a strike-slip border are the keys to atypical subduction.

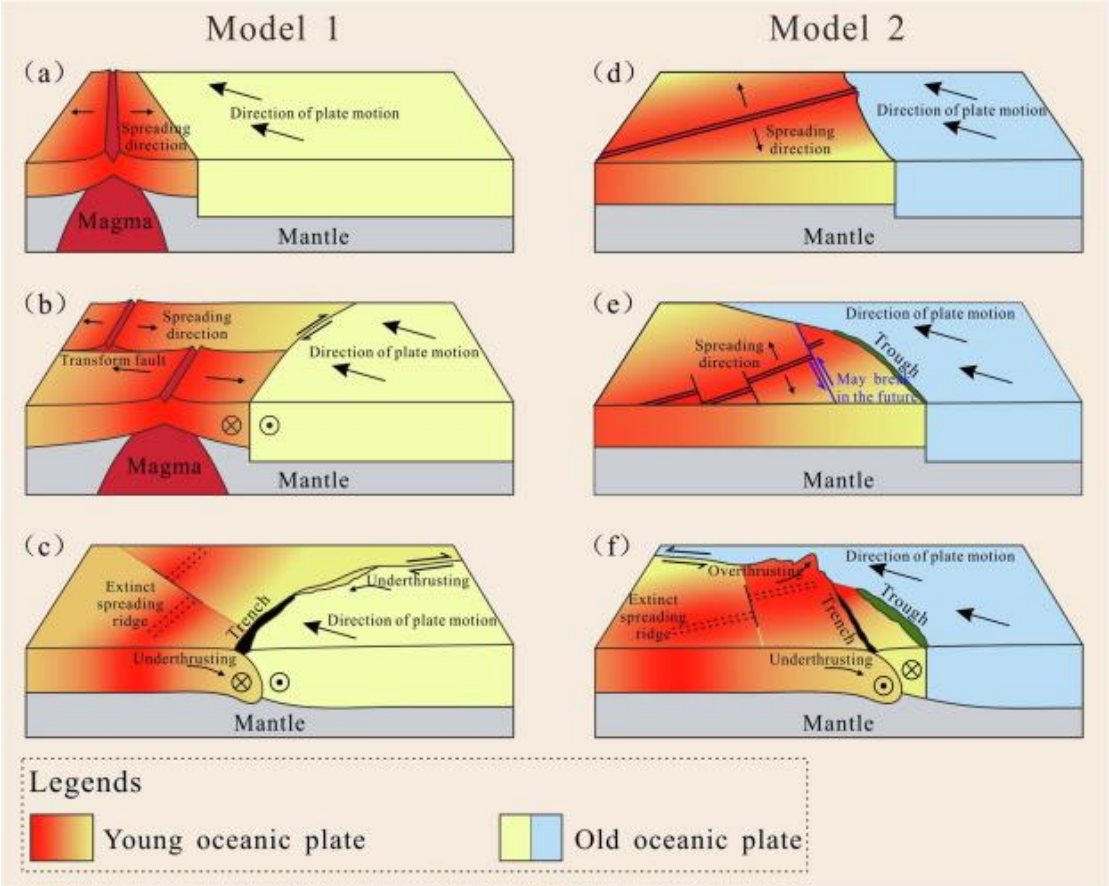

Figure 1. Schematic diagrams of the geological evolutionary model for atypical subductions. Model 1(left column) shows the atypical subduction evolution processes when the plate boundary is parallel to the extinct spreading ridge. (a) The young plate begins to spread in the W–E direction, and the older plate moves along the NW toward the younger plate. (b) As the Euler pole of the plate boundary migrates southward, the motion at the border becomes progressively more strike-slip. (c) With the relative motion of the old and new plates, the transpression stress increases south of the plate boundary, leading to the young plate subducting underneath the old plate. Model 2 (right column) shows the atypical subduction evolution processes when the plate boundary is perpendicular to the extinct spreading ridge. (d) The young plate begins to spread in an NW–SE direction accompanied by clockwise rotation, and the old

plate moves in the NW direction toward the young plate. (e) During the early stages of relative motion of the two plates, a trough serves as a plate boundary. (f) The mid-ocean ridge stops spreading, and subduction of the young plate underneath the old plate occurs along another transform fault, forming a new plate boundary. The red–yellow–blue colors indicate the increasing plate age.

3. 轨道尺度植被动态反馈导致了中国北方全新世降水的减少

翻译人：杨会会 11849590@mail.sustech.edu.cn

Li X Z, Liu X D, Pan Z T, et al., ***Orbital-scale dynamic vegetation feedback caused the Holocene precipitation decline in northern China[J].*** *Communications earth & environment, 2022,3,257*

https://doi.org/10.1038/s43247-022-00596-2

摘要：基于指标重建的中国北方降水在全新世中期(7800-5300 年 BP)出现峰值，随后呈下降趋势，直至今日。大多数研究将这种下降归因于北半球夏季日照减少和东亚夏季风减弱。然而，干燥机制的细节仍然难以捉摸。在这里，我们通过两个瞬态实验来探索中国北方干旱趋势的驱动因素，一个包括动态植被，另一个没有。有动态植被的实验成功地捕捉到了中全新世早期降水的小幅增加和中全新世晚期降水的快速下降，而没有动态植被的实验没有预测到降水的变化。具体而言，在动态植被试验中，植被覆盖随时间的增加，导致约 7800 年 BP 以后的蒸散发和感热增加，从而减少对流降水。我们认为植被动态在全新世降水的长期趋势中起着重要的调节作用。

ABSTRACT: Proxy-based reconstructed precipitation in northern China shows a peak in the mid-Holocene (7800-5300 years BP) followed by a declining trend until the present day. Most studies attributed this decline to the decrease in Northern Hemisphere summer insolation and weakening of the East Asian summer monsoon. However, the details of the drying mechanisms still remain elusive. Here we explore the drivers of this drying trend in northern China using two transient experiments, one that includes dynamic vegetation and one that does not. The experiment with dynamic vegetation successfully captured the slight increase in precipitation in the early mid-Holocene as well as the rapid decline of precipitation in the late mid-Holocene, whereas the experiment without dynamic vegetation predicted no change in precipitation. Specifically, in the dynamic-vegetation experiment, vegetation cover increased over time, which led to higher evapotranspiration and sensible heat and thus a reduction in convective precipitation from about 7800 years BP onwards.

We suggest that the dynamics of vegetation played a key role in modulating the long-term trend of precipitation during the Holocene.

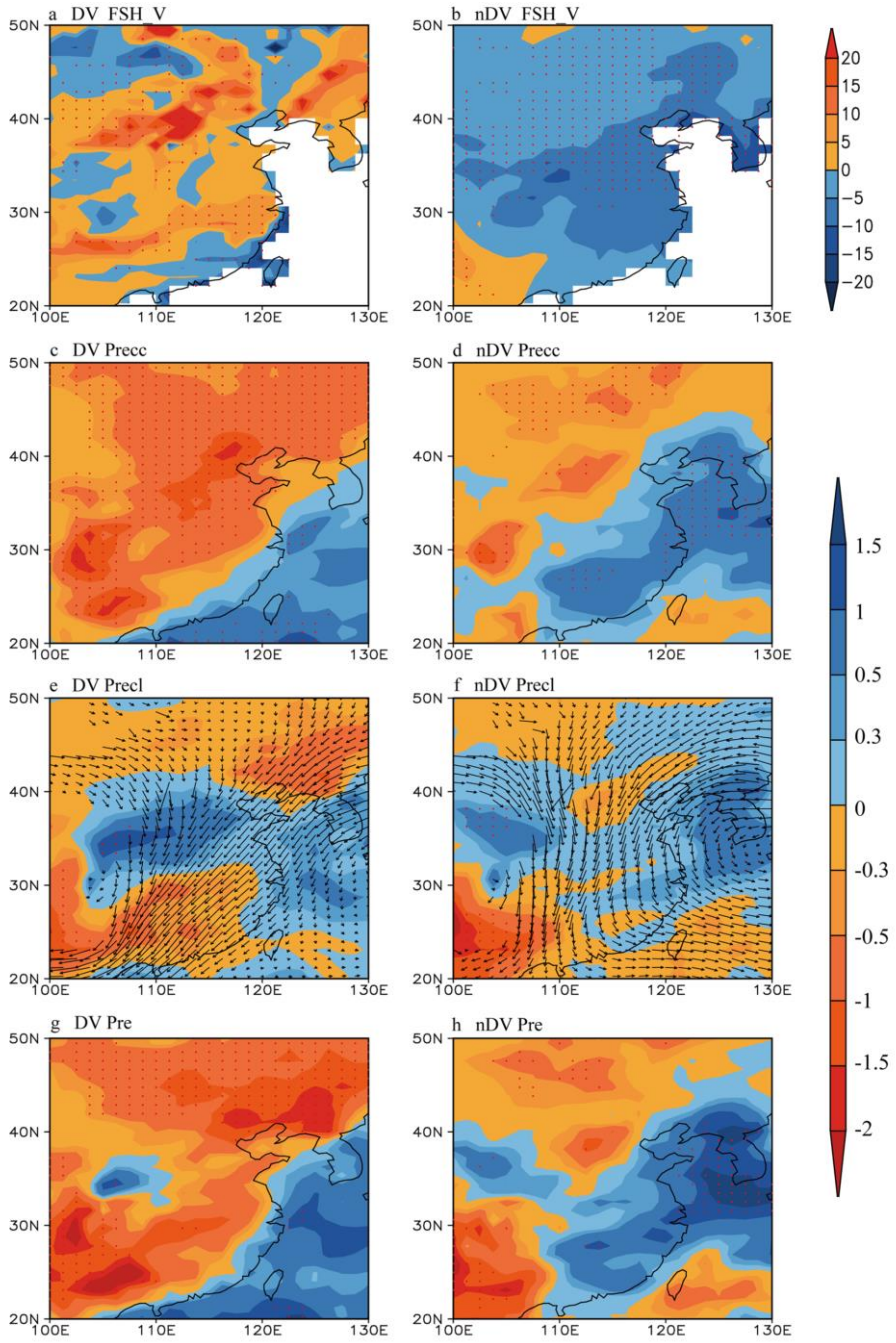

Figure 1. Changes in modern summer sensible heat flux (W/m2) and precipitation (mm/day) compared with early Holocene at 9 kyr BP. a, b DV and nDV simulated FSH_V; c–h Same as a, b but for convective precipitation (Precc), stratiform precipitation (Precl) and total precipitation (Pre), respectively. e, f also show JJA wind field changes at 850 hPa. These figures are generated using GrADS v1.5.1.12.

4. 气候变化增加了加州发生特大洪水的风险

翻译人：曹伟 11930854@qq.com

Huang X, Swain D. ***Climate change is increasing the risk of a California megaflood*** *[J].* ***Science Advances****, 2022, 8(31), abq0995.*

https://www.science.org/doi/10.1126/sciadv.abq0995

摘要：尽管最近发生了严重干旱，但加利福尼亚面临严重洪水的风险被广泛低估。本研究中我们结合气候模型数据和高分辨率天气模型，研究了能够导致“特大洪水”条件的“可能最坏情况”极端风暴序列的物理特征。使用大型地球系统集合模型的数据，我们发现气候变化已经使发生灾难性洪水事件的可能性增加了一倍，但由于持续变暖，未来可能会有更大的增加。我们进一步发现，在未来极端风暴情景下，由于降水率增加和雪覆盖率减少，内华达山脉的径流量将比历史值高出 200 - 400%。这些发现对洪水和应急管理有直接影响，对减灾和气候适应活动也有更广泛的影响。

ABSTRACT: Despite the recent prevalence of severe drought, California faces a broadly underappreciated risk of severe floods. Here, we investigate the physical characteristics of “plausible worst case scenario” extreme storm sequences capable of giving rise to “megaflood” conditions using a combination of climate model data and high-resolution weather modeling. Using the data from the Community Earth System Model Large Ensemble, we find that climate change has already doubled the likelihood of an event capable of producing catastrophic flooding, but larger future increases are likely due to continued warming. We further find that runoff in the future extreme storm scenario is 200 to 400% greater than historical values in the Sierra Nevada because of increased precipitation rates and decreased snow fraction. These findings have direct implications for flood and emergency management, as well as broader implications for hazard mitigation and climate adaptation activities.

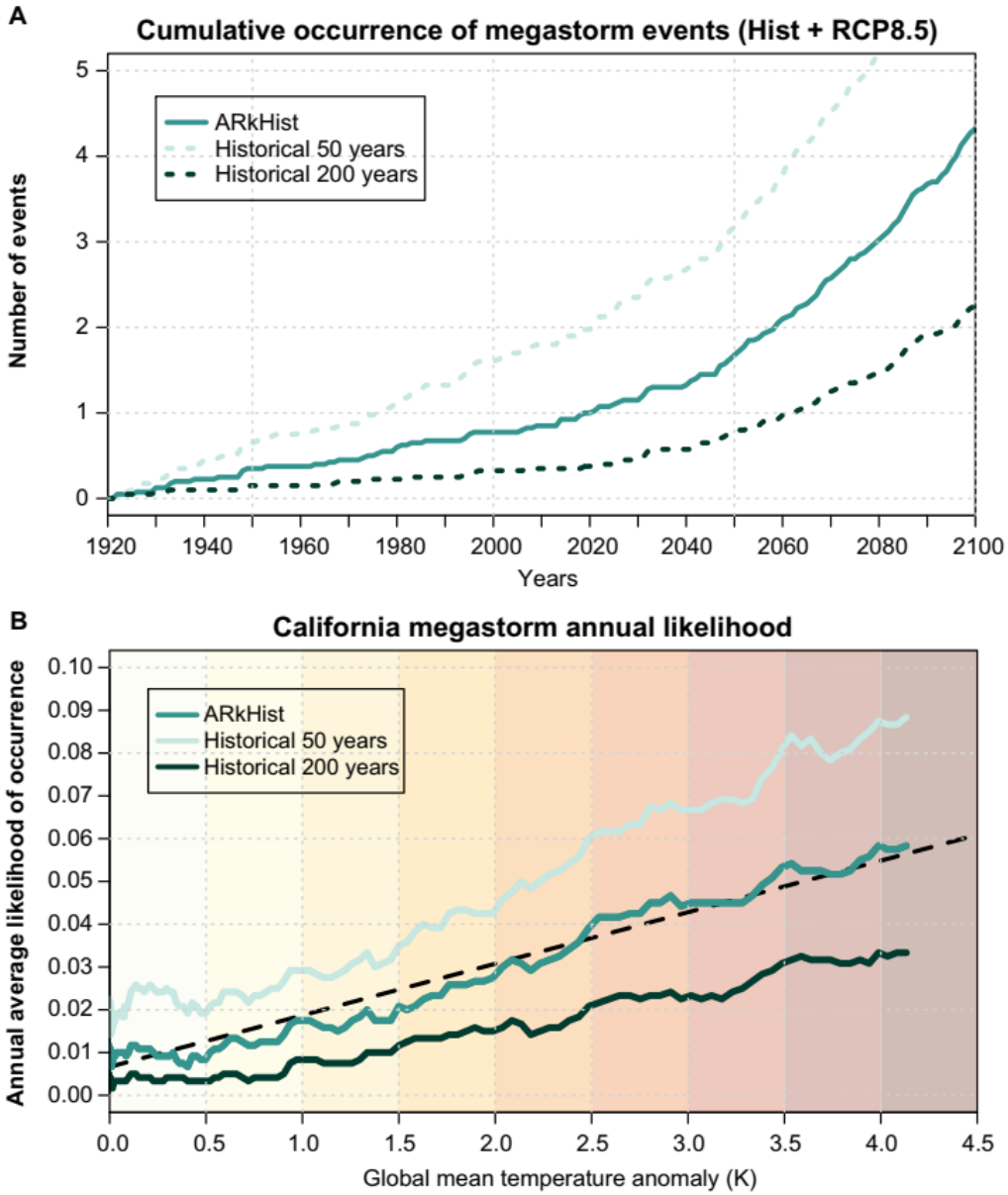

Figure 1. Climate change and California megastorm risk. (A) Cumulative occurrence of extreme 30-day precipitation accumulations on a California statewide basis as simulated by the CESM1-LENS ensemble. The three blue-green curves denote cumulative occurrence of events equal or greater in magnitude to the ARkHist scenario, as well as for events with approximate RIs of 50 and 200 years. Data are drawn from the historical CESM1-LENS simulations for 1920-2005 and from the RCP8.5 scenario for 2006-2100. (B) Annual likelihood of extreme 30-day cumulative precipitation events as a function of projected global mean surface temperature (GMST; K) anomaly across the 40-member ensemble. Blue-green curves correspond to definitions in (A). GMST anomaly is defined relative to a baseline calculated from the CESM1-LENS preindustrial control run, and both annual likelihood and GMST are smoothed on a 30-year running mean basis.

5. 中亚干旱地区全新世湿度变化：重新评估和调和

翻译人：李海 12031330@mail.sustech.edu.cn

Chen S, Chen J, Lv F, et al. ***Holocene moisture variations in arid central Asia: Reassessment and reconciliation*** *[J]. Quaternary Science Reviews, 2022, 297: 107821.*

https://doi.org/10.1016/j.quascirev.2022.107821

摘要： 过去二十多年里对中亚干旱地区全新世水汽变化已经开展了大量研究。然而，这些记录在长期变化上呈现出相互矛盾的结果。此外，为调和不同记录相互矛盾的结果而提出的假设都未能解决这一问题。因此，迫切需要一项整合中亚干旱地区所有高质量记录的研究，以解决这些重建记录相互矛盾的原因（例如指标解释、地貌北京、季节性降水）。作者整理里 36 个有可靠年代学资料的全新世中亚干旱地区的湿度演化记录。综合结果显示了全新世期间长期湿润趋势（31 个记录），而具有不同趋势的记录主要来自于阿尔泰山脉的孢粉和石笋 $\delta^{18}O$ 记录。阿尔泰山脉的孢粉重建的古降水变化可能是受不同海拔地区温度变化的影响。$\delta^{18}O$ 主要受到水汽来源和运输途径的影响，这些因素会影响 $\delta^{18}O$ 作为区域湿度指标的可靠性。去除不确定的指标记录之后，剩下的结果均表现出较为一致的变化趋势，即长期湿润的趋势。因此，作者认为相互矛盾的结果是由指标的不确定性造成的。最后，通过初步梳理中亚干旱地区全新世水汽、同位素、温度和植被变化特征，提出了该区域全新世水-气候-生态系统循环演化的可能框架。

ABSTRACT: During the past two decades there have been numerous studies of Holocene moisture variations in arid central Asia (ACA). However, these available records show contradictory results regarding the long-term trends. Moreover, most hypotheses that have been proposed to reconcile contradictory interpretations have failed to resolve the inconsistencies. Therefore, an up-to-date and comprehensive study incorporating all published high-quality records from the whole of ACA is urgently needed to determine the potential reasons (such as proxy interpretations, geomorphological context, precipitation seasonality) for these contradictory moisture reconstructions. We present a compilation of 36 records of the Holocene moisture evolution of ACA that are supported by reliable

chronologies. The compilation reveals an overall long-term wetting trend (31 out of 36 records) during the Holocene, and it also shows that the records with inconsistent variations were based mainly on pollen assemblages from the Altai Mountains and on stalagmite $\delta^{18}O$ records. The complex patterns of pollen-based precipitation reconstructions from the Altai Mountains can at least partly be attributed to the varying influences of temperature on vegetation change at different elevations. Additionally, the stalagmite $\delta^{18}O$ records were significantly affected by the moisture source and water vapor transport pathways, which adversely affected their reliability as a direct regional moisture indicator. After excluding the records based on ambiguous proxies, we found almost no significant differences between the long-term moisture trends in the remaining records. Therefore, we suggest that the previous contradictory moisture reconstructions are caused mainly by proxy ambiguity. Finally, by preliminarily reconciling the trends of moisture evolution, isotopic variations, temperature changes, and vegetation dynamics in ACA, we attempt to present a possible framework of the circulation-hydroclimate-ecosystem evolution in ACA during the Holocene.

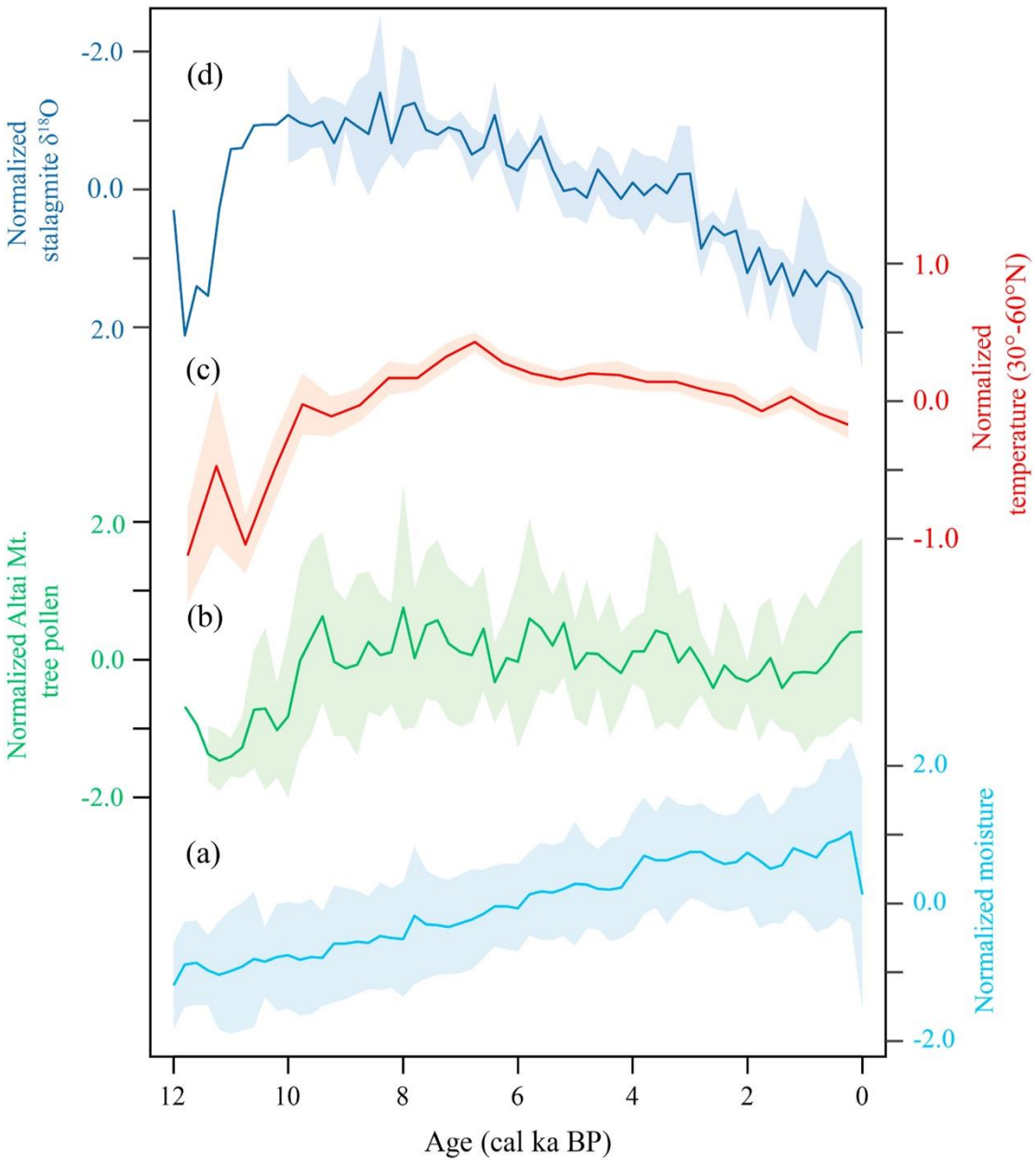

Figure 1. Comparisons of synthesis records from the ACA. (a) The synthesized moisture record based on the remaining 27 moisture records in Table 3. (b) The synthesized forest development record based on six records with temperature passing the significance test (Sites 29–34) from the high-elevation Altai Mountains. (c) Mid-latitude (30°N–60°N) temperature variation during the Holocene (Kaufman et al., 2020). (d) The synthesized stalagmite $\delta^{18}O$ record from three caves (Sites 4, 13, 19). Due to the absent of data, the error estimations of synthetical stalagmite $\delta^{18}O$ record during 12–10 ka were absent. The synthetical records were calculated based on the Z-score normalization method.

6. 晚冰期南大洋海洋碳再分布和释放的证据

翻译人：张亚南 zhangyn3@mail.sustech.edu.cn

Iwasaki S, Lembke-Jene L, Nagashima K, et al. ***Evidence for late-glacial oceanic carbon redistribution and discharge from the Pacific Southern Ocean*** *[J] Nature Communications, 2022, 13: 6250.*

https://doi.org/10.1038/s41467-022-33753-4

摘要：南大洋深水环流在全球碳循环中起着至关重要的作用。在地质时间尺度上，沿智力边缘的上升流可能促进了冰消期大气二氧化碳的上升，但却几乎没有定量的碳循环证据存在。文中，我们开发了一种 X 射线显微计算机断层扫描方法（X-ray Micro-Computer-Tomography），根据有孔虫壳体的溶解去评估过去碳酸根离子浓度（$[CO_3^{2-}]$）。来自亚南极东南太平洋沉积物的岩心结果表明，在末次冰盛期和冰消期深海$[CO_3^{2-}]$发生了显著变化。我们提供了 LCDW 在冰消期早期（15-19 ka）$[CO_3^{2-}]$增加的证据。从太平洋向大西洋传输的这种低碳深水，显著降低了南大洋的碳储库，突出了太平洋-南大洋深水重新分配的变化对晚冰期大洋碳储库的改变，以及随后冰消期海洋-大气间的 CO_2 转移具有重要的作用。

ABSTRACT: Southern Ocean deep-water circulation plays a vital role in the global carbon cycle. On geological time scales, upwelling along the Chilean margin likely contributed to the deglacial atmospheric carbon dioxide rise, but little quantitative evidence exists of carbon storage. Here, we develop an X-ray Micro-Computer-Tomography method to assess foraminiferal test dissolution as proxy for paleo-carbonate ion concentrations ($[CO_3^{2-}]$). Our subantarctic Southeast Pacific sediment core depth transect shows significant deep-water $[CO_3^{2-}]$ variations during the Last Glacial Maximum and Deglaciation (10-22 ka BP). We provide evidence for an increase in $[CO_3^{2-}]$ during the early-deglacial period (15-19 ka BP) in Lower Circumpolar Deepwater. The export of such low-carbon deep-water from the Pacific to the Atlantic contributed to significantly lowered carbon storage within the Southern Ocean, highlighting the importance of a dynamic Pacific-Southern Ocean deep-water reconfiguration for shaping late-glacial oceanic carbon storage, and subsequent deglacial oceanic-atmospheric CO_2 transfer.

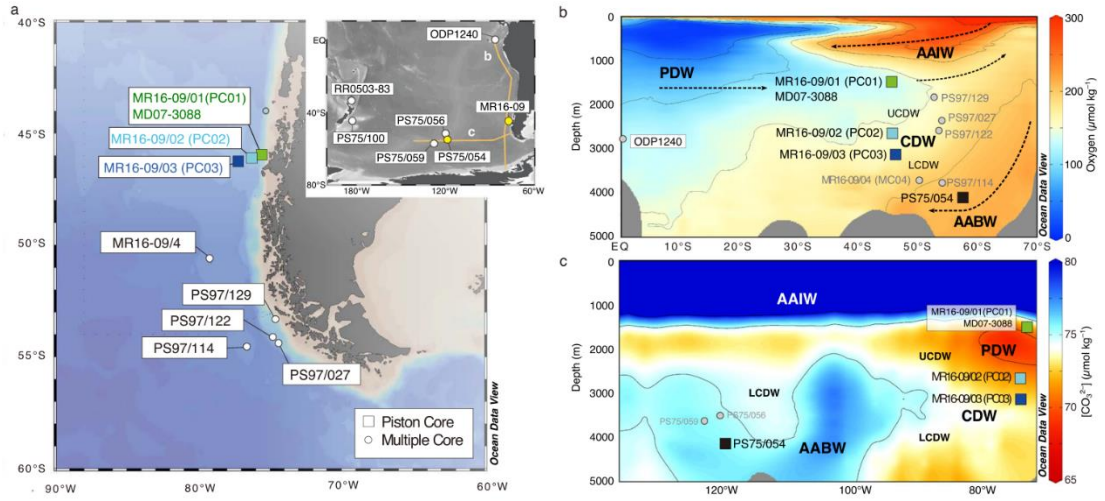

Figure 1. Cores location and study area. a Location of piston cores of MR16-09 (PC01: 46° 04′S, 75° 41′W; 1537m water depth, PC02: 46° 04′S, 76° 32′W; 2787m water depth, PC03: 46° 24′S, 77° 19′W; 3074m water depth), and location of multiple cores analyzed in this study. The enlarged map shows locations of PS75/054−1(56°S, 115°W, 4085m) and core sites referred to in this study. b Cross-sections of oxygen concentration (µmol kg^{-1}) along ~80°W and c seawater [CO_3^{2-}] (µmol kg^{-1}) along ~47°S based on the data from Global Ocean Data Analysis Project (GLODAP). The distribution of principal water masses (PDW Pacific Deep Water, AAIW Antarctic Intermediate Water, AABW Antarctic Bottom Water, CDW Circumpolar Deep Water) is shown. Map and sections generated using Ocean Data View.

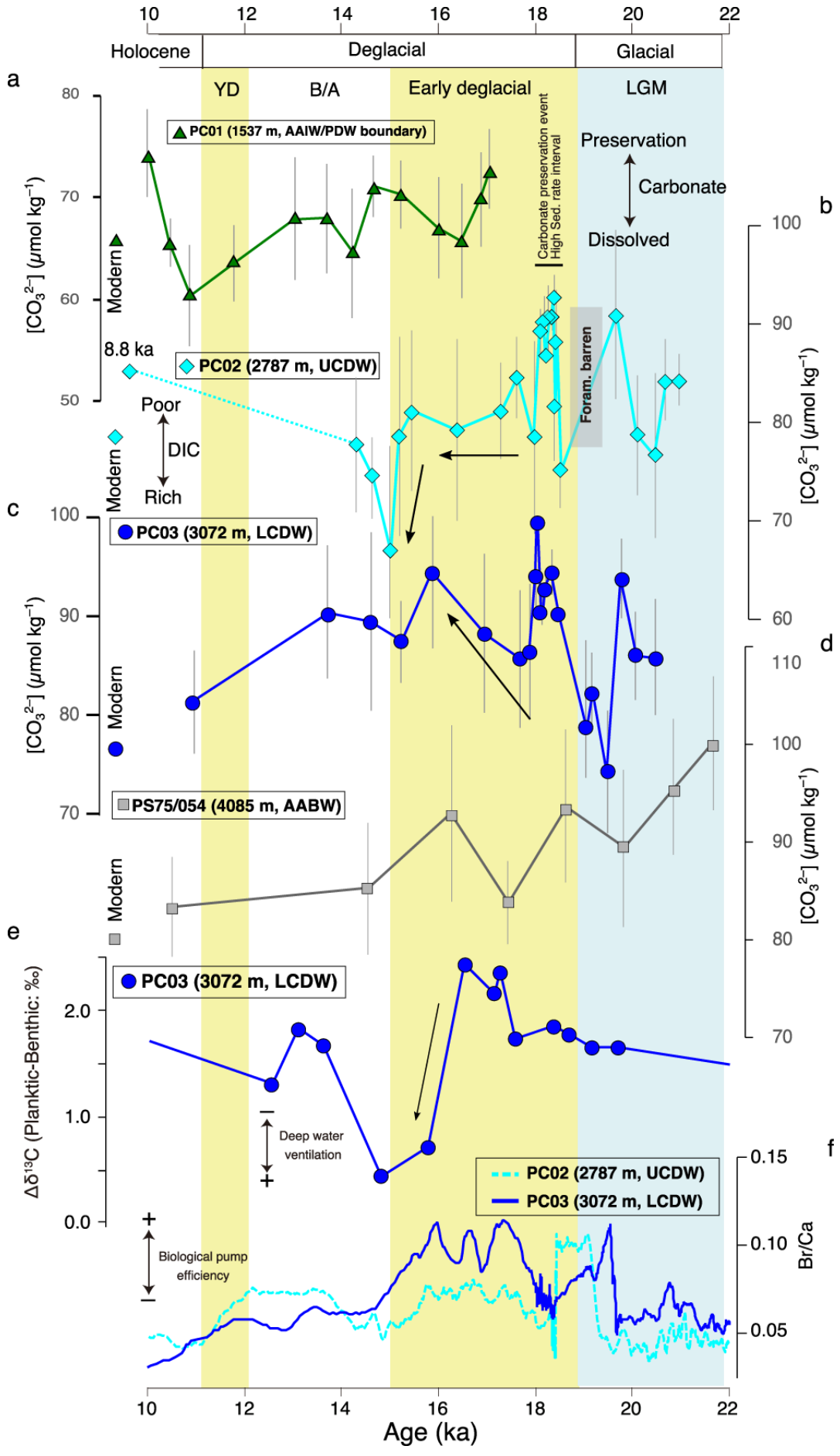
10
12
14
16
18
20
22
Holocene
Deglacial
Glacial
YD
B/A
Early deglacial
LGM
a
b
c
d
e
f
PC01 (1537 m, AAIW/PDW boundary)
Carbonate preservation event
High Sed. rate interval
Preservation
Carbonate
Dissolved
[CO3 2−] (μmol kg−1)
Modern
8.8 ka
PC02 (2787 m, UCDW)
Foram. barren
Poor
DIC
Rich
PC03 (3072 m, LCDW)
PS75/054 (4085 m, AABW)
Δδ13C (Planktic-Benthic: ‰)
Deep water ventilation
Biological pump efficiency
Br/Ca
Age (ka)

Figure 2. Reconstruction of deep-water [CO_3^{2-}] during 10–22 ka BP. a PC01, b PC02, c PC03, and d PS75/054. e Difference in stable carbon isotope ratio ($\Delta\delta^{13}C$) between planktic and benthic foraminifera, and f Br/Ca ratio in PC02 and PC03. YD Younger Dryas, BA Bølling-Allerød, LGM Last Glacial maximum, DIC Dissolved inorganic carbon, UCDW Upper Circumpolar Deep Water, LCDW Lower Circumpolar Deep Water.

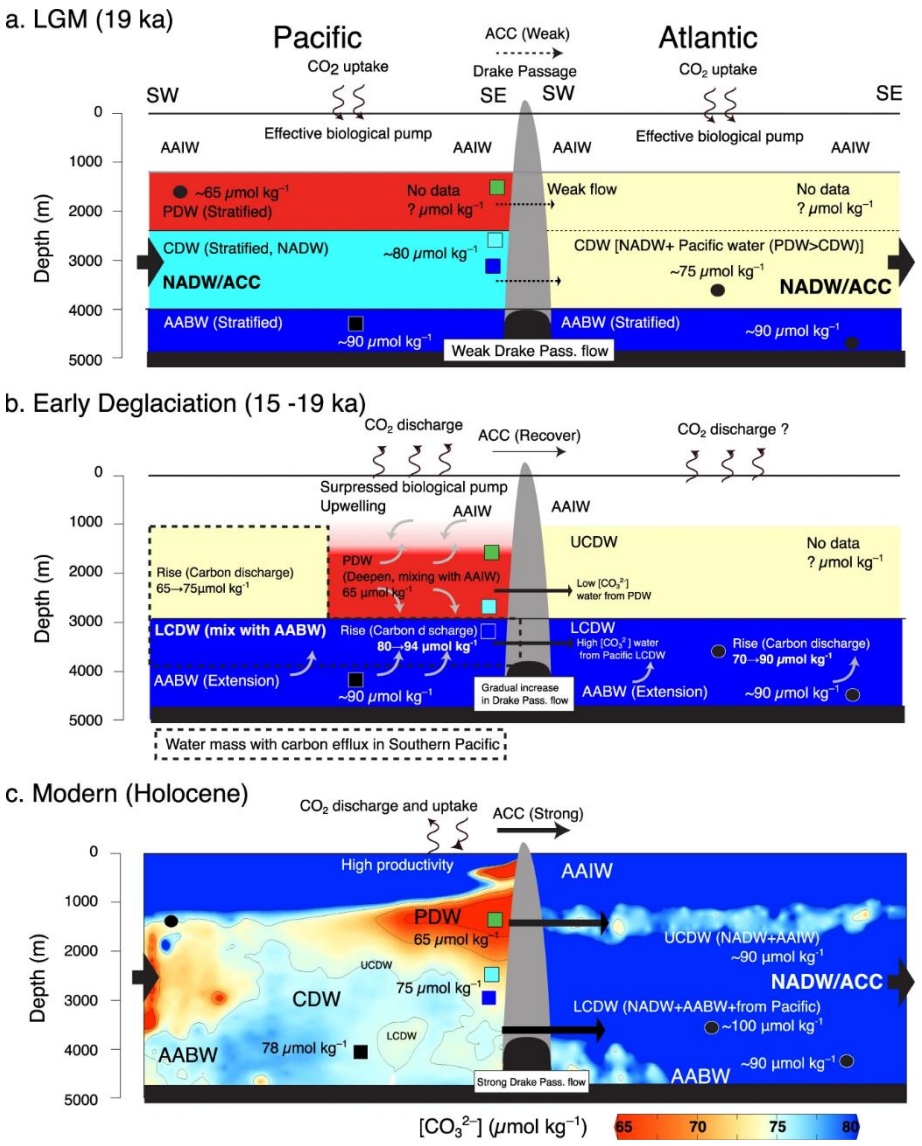

Figure 3. Schematic illustration of water column structure in the Southern Pacific and the Southern Atlantic at the end of LGM, the early deglacial, and Modern condition. a LGM (Last Glacial Maximum, 19 ka BP): characterized by strong deep-water stratification, weak Antarctic Circumpolar Current (ACC), weak Drake Passage flow, and strong Atlantic meridional overturning circulation (AMOC). b The early deglaciation (15–19 ka BP): break up of deep-water stratification,

strengthening of ACC, strengthening of Drake Passage flow, and weakening or stop of AMOC. c Modern condition: moderate mixing of deep-water, Strong ACC, Strong Drake Passage flow, and strong AMOC. West-East transect of [CO32−] at ~30°S is based on the modern data from GLODAP. Section generated using Ocean Data View.

7. 在不同的时间尺度上是否存在稳定的地球系统反馈

翻译人：张靖宇 zhangjy6@sustech.edu.cn

Constantin.W. Arnscheidt and Daniel H. Rothman. ***Presence or absence of stabilizing Earth system feedbacks on different time scales*** *[J]. Science Advance, 2022, 8, eadc9241.*

https://www.science.org/doi/10.1126/sciadv.adc9241

摘要：地球气候在地质时间尺度上是如何稳定的，这个问题对于理解地球的历史、人为气候变化的长期结果和行星的宜居性非常重要。在这里，我们量化了过去全球温度波动在几百到几千万年的时间尺度上的典型振幅，并利用它来评估气候系统中是否存在长期稳定的反馈作用。在 4 到 400ka 的时间尺度上，波动没有随着时间尺度而增长，这表明像假设的“风化反馈”这样的稳定机制在这个系统中发挥了主导控制作用。波动在更长的时间尺度上增长，可能是由于构造或生物驱动的变化，使风化作用成为气候强迫和反馈。这些较慢的波动没有显示出被抑制的证据，这意味着可能仍然在维持地球的长期宜居性方面发挥了不可忽视的作用。

ABSTRACT: The question of how Earth’s climate is stabilized on geologic time scales is important for understanding Earth’s history, long-term consequences of anthropogenic climate change, and planetary habitability. Here, we quantify the typical amplitude of past global temperature fluctuations on time scales from hundreds to tens of millions of years and use it to assess the presence or absence of long-term stabilizing feedbacks in the climate system. On time scales between 4 and 400 ka, fluctuations fail to grow with time scale, suggesting that stabilizing mechanisms like the hypothesized “weathering feedback” have exerted dominant control in this regime. Fluctuations grow on longer time scales, potentially due to tectonically or biologically driven changes that make weathering act as a climate forcing and a feedback. These slower fluctuations show no evidence of being damped, implying that chance may still have played a nonnegligible role in maintaining the long-term habitability of Earth.

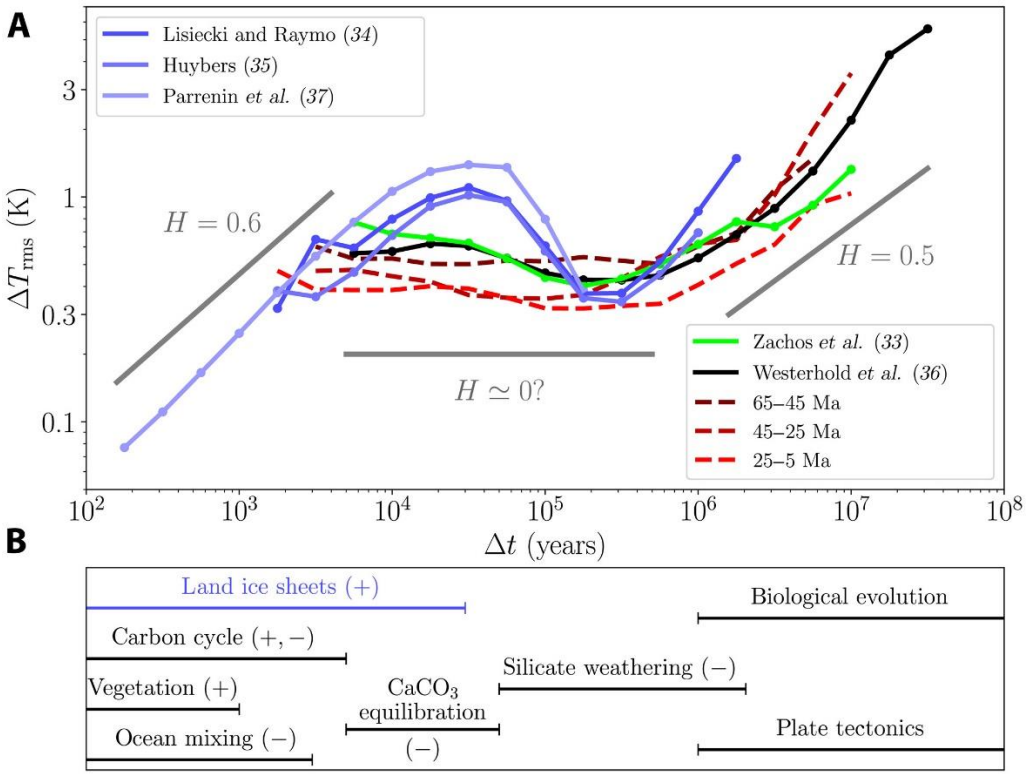

Figure 1. Temperature fluctuations and feedback mechanisms. (A) Root mean square temperature fluctuations ΔTrms as a function of time scale Δt (Materials and Methods) for five different paleotemperature time series and three nonoverlapping segments of the data from. Power-law scalings with fixed exponents H are shown as guides for interpretation. On time scales below about 4 ka and above about 400 ka, fluctuations behave similarly to the random walk (H≃ 0.5; Eq. 1). In contrast, fluctuations do not grow with time scale in the intermediate regime, suggesting that stabilizing feedbacks were dominant here. The peak at ∼30 ka in the Plio-Pleistocene data (blue) and the strongly decreasing regime beyond it are likely signatures of glacial-interglacial variability. (B) Approximate time scales of relevant Earth system processes (see Materials and Methods for details). The symbols + and - indicate positive (destabilizing) and negative (stabilizing) feedbacks, respectively. The land ice sheet feedback is colored blue to emphasize that it is primarily relevant only after the onset of Northern Hemisphere glaciation ∼3 Ma ago.

8. 中更新世海平面变化与弗雷泽岛和大堡礁形成之间的联系

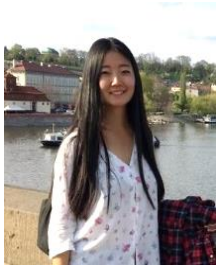

翻译人：张琪 zhangq7@sustech.edu.cn

Ellerton D, Rittenour T, Shulmeister J, et al, ***Fraser Island (K'gari) and initiation of the Great Barrier Reef linked by Middle Pleistocene sea-level change*** *[J]. Nature Geoscience, 2022.*

https://doi.org/10.1038/s41561-022-01062-6

摘要：澳大利亚东部海岸线独特的海岸地貌和向北延绵广阔的沿岸漂移系统，受第四纪稳定且长期的构造历史的影响。然而，对弗雷泽岛和大堡礁这两个引人注目的景观特征形成时间和驱动力我们仍然知之甚少。本文中，作者使用光释光法和古地磁测年法对弗雷泽岛（世界上最大的沙岛）和邻近的昆士兰州东南部库罗拉沙群广阔的沙丘形成进行了约束。作者们发现它们都形成于 1.2 Ma 到 0.7 Ma 之间，处于中更新世过渡期全球气候重构中。它们的形成是海平面波动幅度增大的直接结果，且与全球冰量增加有关，这样就会对以往储存在大陆架上的沉积物进行了重新分配。弗雷泽岛的不断发展大大减少了岛北部大陆架沉积物的供应。因此促进了大堡礁南部和中部广阔的珊瑚礁的形成，这也是大堡礁形成的必要前提。这种海岸沉积系统的重大重组可能不是澳大利亚东部所独有的，此类研究也适用于其他被动边缘海岸线。

ABSTRACT: The eastern Australia coastline is characterized by impressive coastal landforms and an extensive northward-moving longshore drift system that have been influenced by a stable, long-term tectonic history over the Quaternary period. However, the timing and drivers of the formation of two conspicuous landscape features-Fraser Island (K'gari) and the Great Barrier Reef-remain poorly understood. Here we use optically stimulated luminescence and palaeomagnetic dating to constrain the formation of the extensive dunes that make up Fraser Island, the world's largest sand island, and adjacent Cooloola Sand Mass in southeastern Queensland. We find that both formed between 1.2 Ma and 0.7 Ma, during a global climate reconfiguration across the Middle Pleistocene transition. They formed as a direct result of increased amplitude of sea-level fluctuations associated with increasing global ice volume that redistributed previously stored sediment across the

continental shelf. The development of Fraser Island dramatically reduced sediment supply to the continental shelf north of the island. This facilitated widespread coral reef formation in the southern and central Great Barrier Reef and was a necessary precondition for its development. This major reorganization of the coastal sedimentary system is probably not unique to eastern Australia and should be investigated in other passive-margin coastlines.

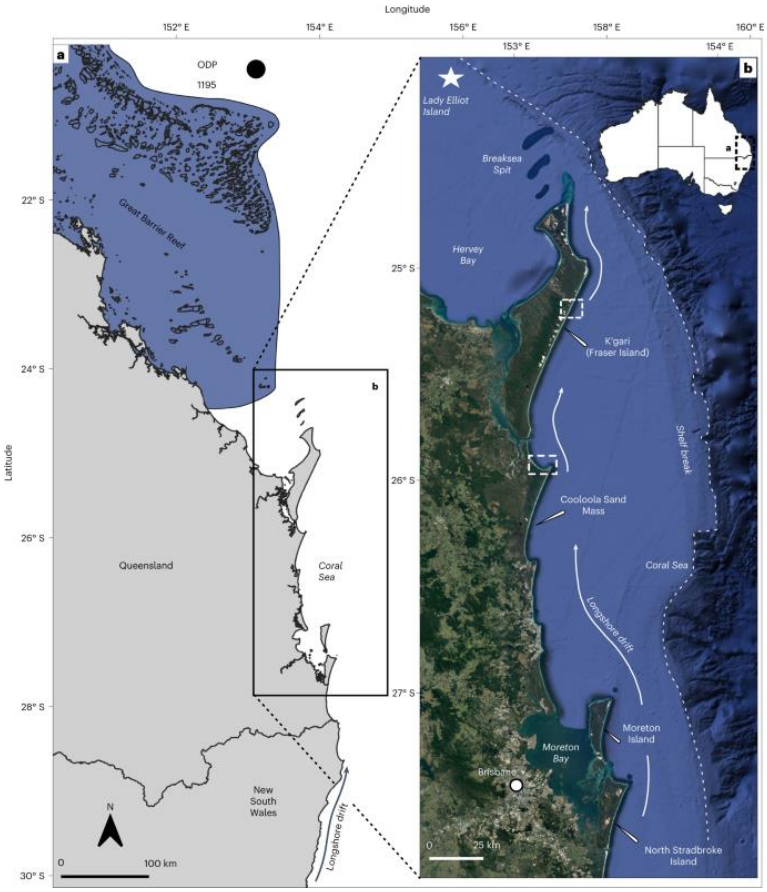

Figure 1. Overview and location map of areas discussed in the text. a, Map of eastern Australia with dominant longshore drift system, the southern GBR and Ocean Drilling Program Site 1195 (ODP 1195). b, Location of Fraser Island, the Cooloola Sand Mass and other areas discussed in the text. The white dashed boxes in b indicate sampling locations for Rainbow Beach (Cooloola) and the Fraser Island cliffs (Fraser Island). The longshore drift system that operates along the coast is indicated, along with Lady Elliot Island, which is the southernmost emergent reef of the GBR. Note the proximity of the continental shelf break to the northern tip of Fraser Island. Longshore sediment transported north of Fraser Island is redirected off the continental shelf and is transported to the abyssal plain.

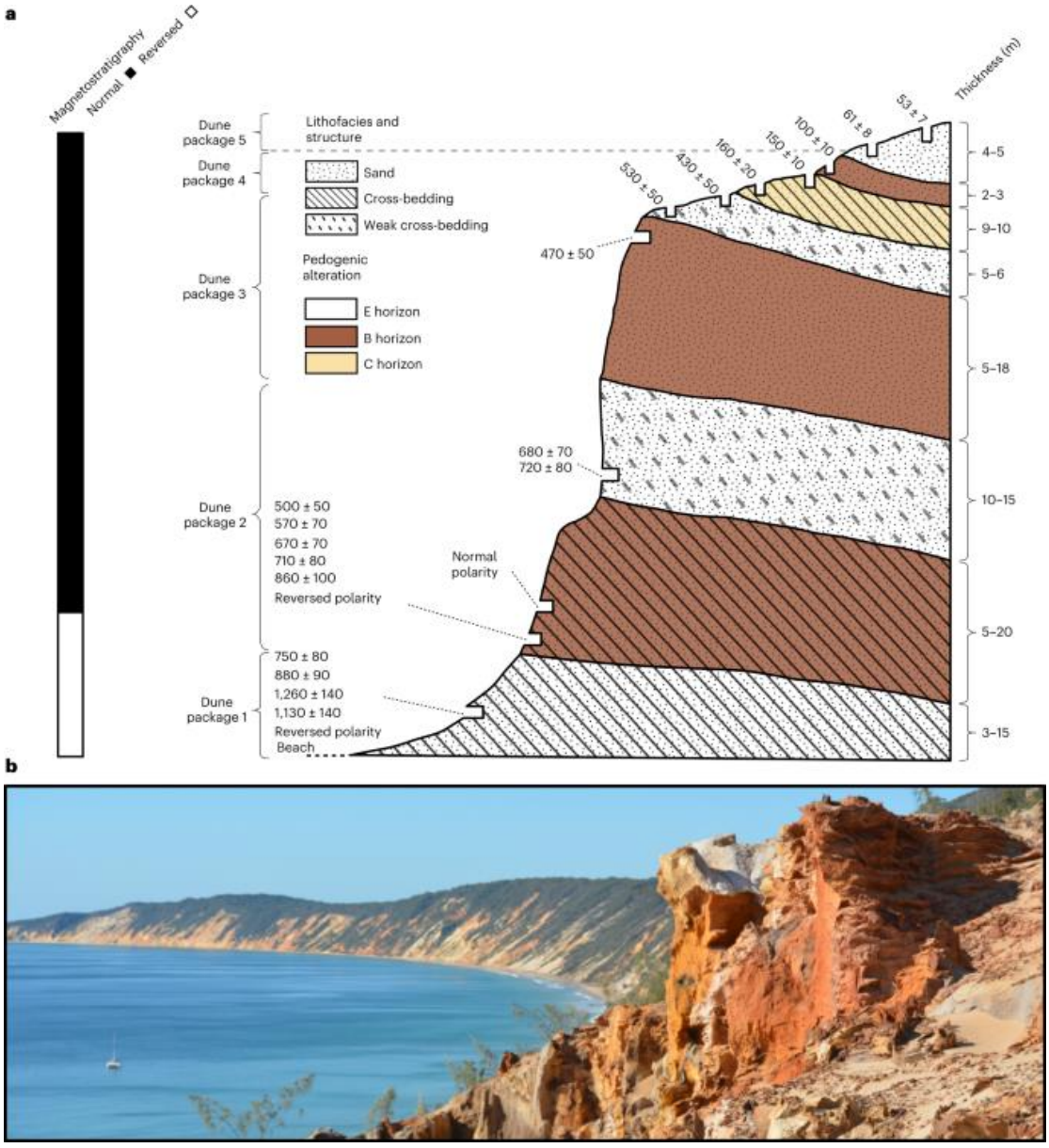

Figure 2. Summary of results for the Cooloola Sand Mass with stratigraphy and chronology. a, Generalized stratigraphy and cross section for Rainbow Beach with OSL ages, palaeomagnetic polarity, soil and stratigraphic packages. For detailed stratigraphic information and sample locations. For stratigraphic and chronological information of the Fraser Island cliffs. b, View of the Rainbow Beach cliffs to the southeast. In the foreground is an example of the ferricrete used for palaeomagnetic analysis. In lower units, thin, less well-developed ferricretes were used for palaeomagnetic analyses.

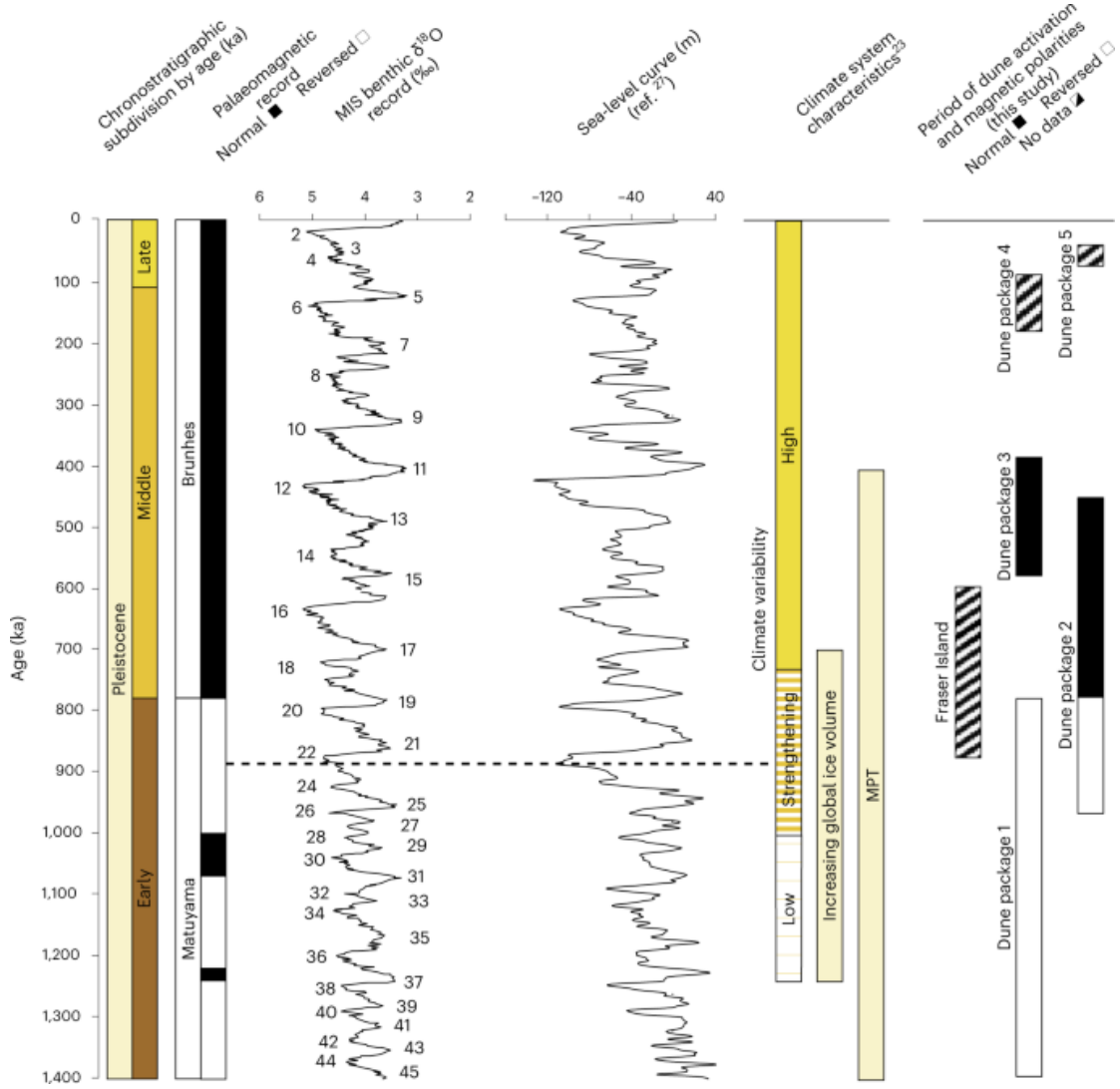

Figure 3. Correlations of geological and marine isotope data with the timing of dune formation at the Cooloola Sand Mass and Fraser Island. The periods of dune activation represent the total spread of ages from each dune package, including uncertainties. Note, however, that dune package 1 (reversed polarity) and the base of dune package 2 (reversed polarity) are constrained by the age of the Matuyama/Brunhes boundary and must be older than 773 ka. The dashed horizontal line indicates the first noteworthy drop to -120 m sea level (MIS 22).

9. 全球热带气旋快速增强的一个潜在解释

翻译人：夏文月 12231072@mail.sustech.edu.cn

Bhatia K., Baker A., Yang W., et al. **A potential explanation for the global increase in tropical cyclone rapid intensification** *[J]. Nature Communications, 2022, 13, 6626.*

https://doi.org/10.1038/s41467-022-34321-6

摘要：热带气旋快速增强事件经常导致破坏性的飓风登陆，因为它们与最强的风暴和预测的最大误差值有关。几十年的热带气旋行为观测数据集最近能够记录几个盆地热带气旋快速增强的上升趋势。然而，全球变暖趋势中强有力的人为信号和加剧趋势的物理驱动因素尚未确定。为了解决这些知识缺口，我们在这里将观测到的增强趋势和热带气旋环境参数与高分辨率全球气候模型模拟的自然变率进行了比较。在多个盆地和全球数据集中，我们发现了增强速率的显著增加，这与人为强迫的正向贡献有关。此外，热带气旋周围的热力环境已变得更有利于增强，气候模型显示人为变暖显著增加了这些变化的可能性。

ABSTRACT: Tropical cyclone rapid intensification events often cause destructive hurricane landfalls because they are associated with the strongest storms and forecasts with the highest errors. Multi-decade observational datasets of tropical cyclone behavior have recently enabled documentation of upward trends in tropical cyclone rapid intensification in several basins. However, a robust anthropogenic signal in global intensification trends and the physical drivers of intensification trends have yet to be identified. To address these knowledge gaps, here we compare the observed trends in intensification and tropical cyclone environmental parameters to simulated natural variability in a high-resolution global climate model. In multiple basins and the global dataset, we detect a significant increase in intensification rates with a positive contribution from anthropogenic forcing. Furthermore, thermodynamic environments around tropical cyclones have become more favorable for intensification, and climate models show anthropogenic warming has significantly increased the probability of these changes.

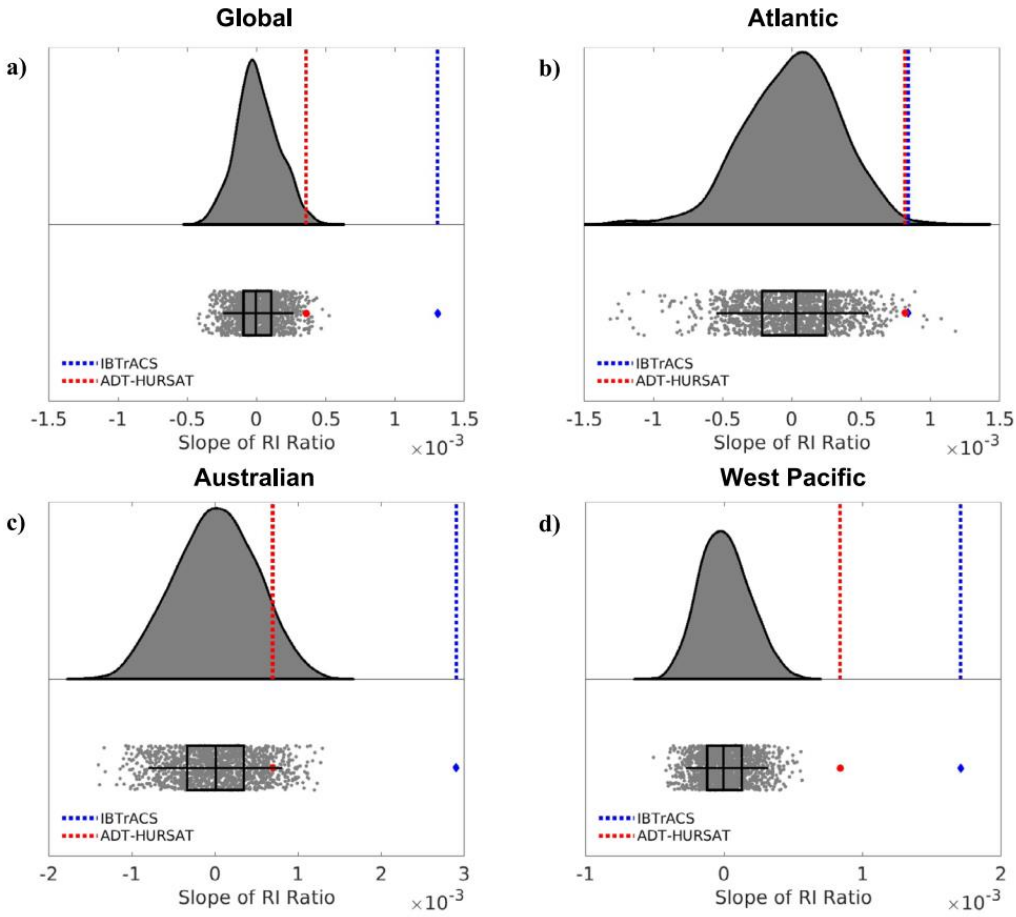

Figure 1. Observed trends in rapid intensification ratio vs. HiFLOR natural variability. Raincloud plots represent the distribution of rapid intensification (RI) ratio slopes in the Quantile Delta Mapping-corrected 1860 HiFLOR control simulation using a half-violin plot (top) and raw jittered data and box-and-whisker plots (bottom) for four basins (a) Global (b) Atlantic (c) Australian (d) West Pacific. Each of the HiFLOR slopes is calculated by applying least squares regression analysis to annual RI ratio values in 1,414 (number of available years reduced by 36) overlapping 36-year periods. The center line of the box represents the median and is bounded by the 25th and 75th percentiles of the data, and the whiskers bracket approximately 95% of the data. IBTrACS and ADT-HURSAT trends in annual mean RI ratio between 1982–2017 are respectively represented in bottom (top) subplot by a blue diamond (blue dotted line) and red circle (red dotted line).

10. 春节期间大规模人类活动变化引发城市热岛变化的城乡梯度

翻译人：聂美娟 12232216@mail.sustech.edu.cn

Zhan W, Liu Z, Bechtel B, et al. ***Urban-rural gradient in urban heat island variations responsive to large-scale human activity changes during Chinese New Year holiday****[J].* ***Geophysical Research Letters,49, e2022GL100689.***

https://doi.org/10.1029/2022GL100689

摘要：春节期间特大城市的大规模人类活动变化会对城市热岛 (UHIs)有显著的影响。然而，城市热岛变化的城乡梯度对人类活动变化的响应机制仍不明确。利用从 3000 多个气象站的气象网络获得的原位地表气温，我们研究表明，在春节假期期间，中国 31 个城市的平均 UHI 强度为 0.52±0.23K，在对照期间为 0.77±0.29K，表示假期 UHII 减少 0.25±0.20K。从城市核心(0.54 K)到城市外围(0.071K)，UHII 的减少幅度更大。我们发现，这些 UHII 的减少在夜间比白天大，在北亚热带和暖温带气候中比在其他气候中更大。这些 UHII 的减少主要由于人为放热的减少。

ABSTRACT: Large-scale human activity changes in megacities during Chinese New Year (CNY) are believed to significantly affect urban heat islands (UHIs). However, the urban-rural gradient in UHI variations responsive to human activity changes in cities remains largely unclear. Using in-situ surface air temperature obtained from a meteorological network that includes 3000-plus stations, we show that the mean UHI intensity (UHII) in 31 Chinese capitals is 0.52 ± 0.23K during the CNY holiday and 0.77 ± 0.29K in the reference period, indicating a UHII reduction of 0.25 ± 0.20K during the holiday. The reduced UHII decreased more from city core (0.54K) to city periphery (0.071K). We find that these UHII reductions were larger at night than during the day and were larger in northern subtropical and warm temperate climates than in other climates. These UHII reductions were mainly attributable to the decline in anthropogenic heat release.

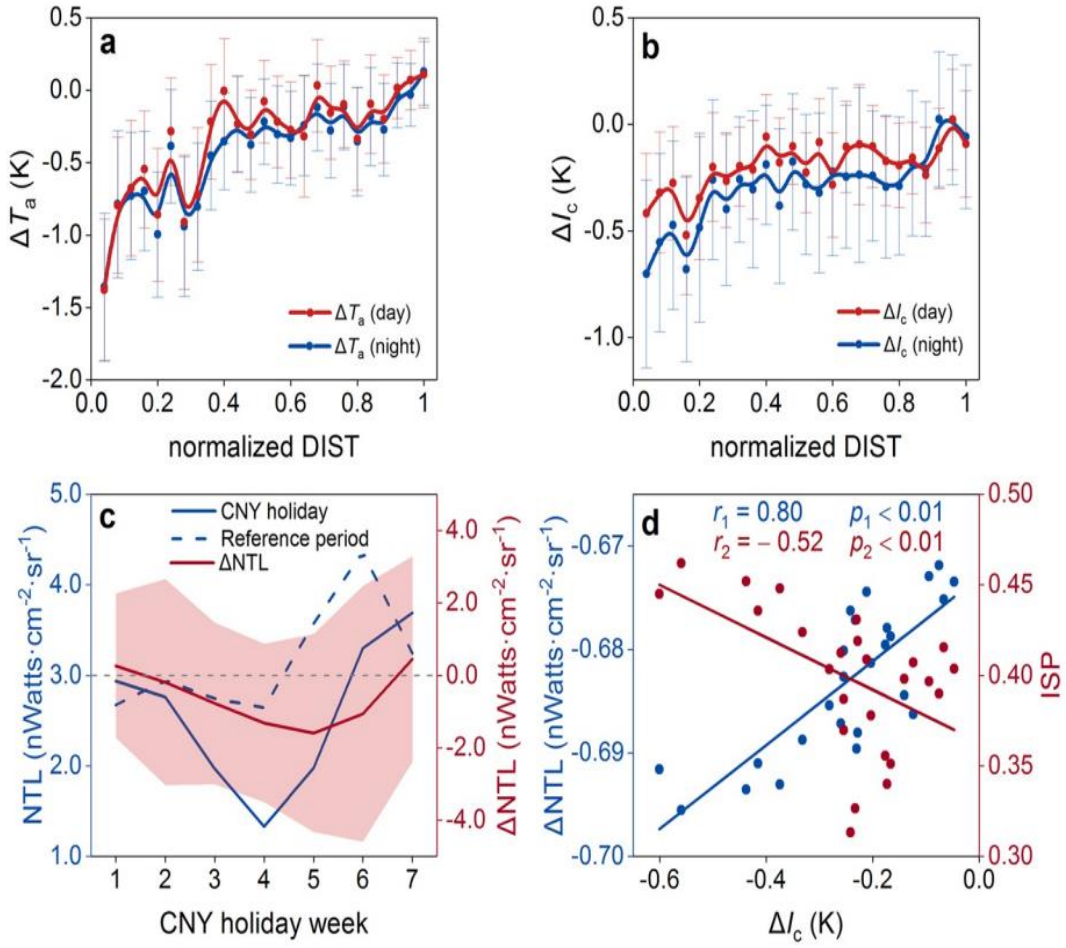

Figure 1. Relationships between change in surface air temperature (SAT) (ΔTa), ΔIc, and night-time light (NTL) to the distance of the measurement station from the city core and day of the Chinese New Year (CNY) holiday week. Comparison of the distance of the measurement station to the city core to day and night-time values of (a) the change in SAT during the CNY holiday period from the reference period (ΔTa) and (b) ΔIc. (c) Daily variation in NTL (ΔNTL) during the CNY holiday week. (d) Comparison of ΔIc to ΔNTL and impervious surface percentage. DIST denotes the distance of station from the city core: we normalized the distances of all urban stations from city cores into 0 to 1, with the maximum distance of each city being set as the radius of its minimum circumcircle.

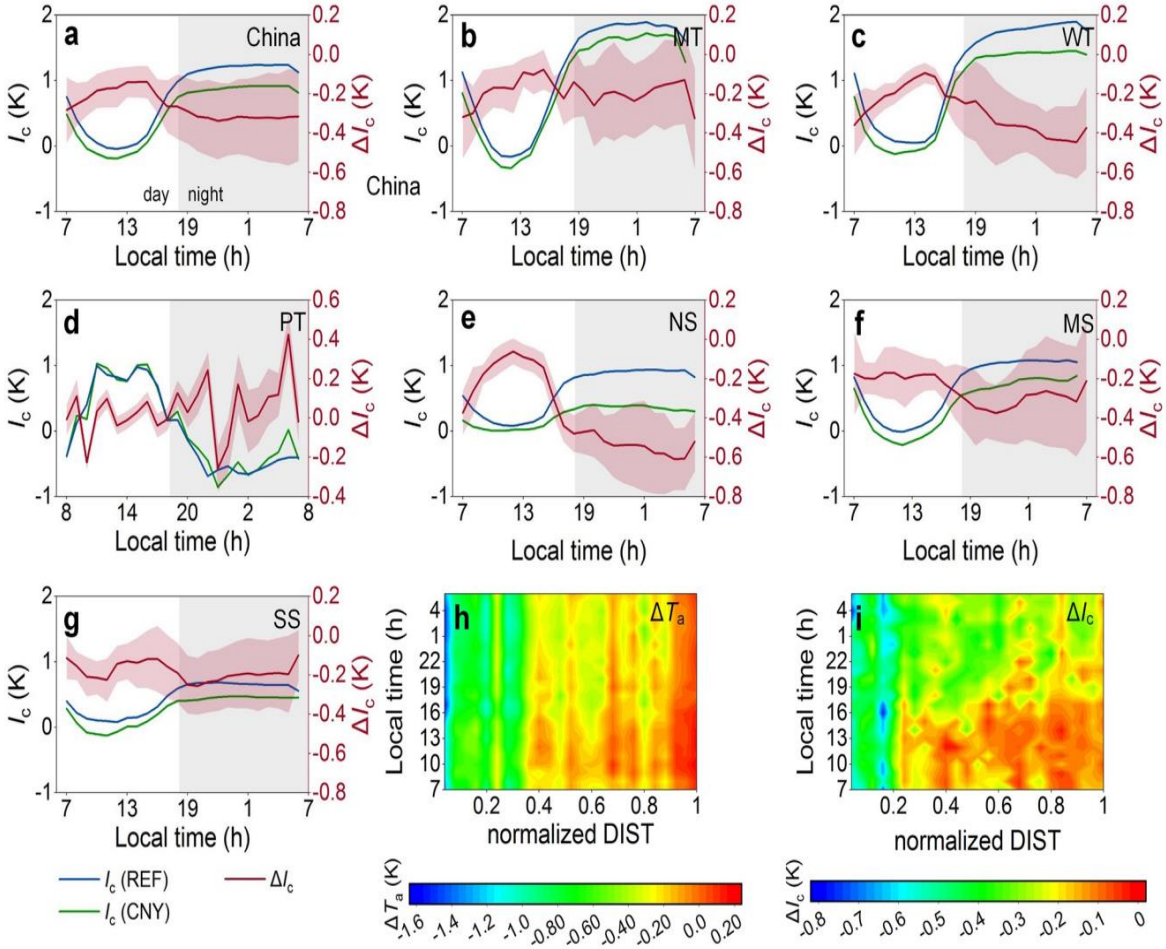

Figure 2. Hourly variations in urban heat island intensity during the CNY holiday (green lines) and the reference period (blue lines), as well as the associated and ΔI_c (red lines). (a) Average values from all the capitals. (b–g) Average values for cities in each climate zone. Hourly variations in (h) ΔT_a and (i) ΔI_c from the city core to the periphery. DIST denotes the distance of the station from the city core.

11. 末次冰消期和全新世期间中层洋流和印度季风风化输入的千年变化

翻译人：刘宇星 liuyx2018@mail.sustech.edu.cn

Yu Z, Colin C, Wilson D J, et al. ***Millennial variability in intermediate ocean circulation and Indian monsoonal weathering inputs during the last deglaciation and Holocene****[J]. Geophysical Research Letters, 2022: e2022GL100003.*

https://doi.org/10.1029/2022GL100003

摘要：海洋环流与季风系统在轨道到次千年时间尺度上的关系是气候系统的一个重要但缺乏研究的组成部分。在这里，我们利用北印度洋中层深度的有孔虫和碎屑钕(Nd)同位素记录，提供了新的证据，表明季风驱动的风化输入和来自南大洋的水团平流影响了该地区过去的海水 Nd 同位素变化.我们的研究结果表明，在最后一次冰消期期间，印度夏季风减弱与向北南极中层水(AAIW)平流增强同时发生，反映了强烈的半球间耦合。相比之下，早全新世的特点是季风强度增强，但 AAIW 流入量持续强劲，表明存在相反意义的关系。这些不同的半球间关系表明全球大气-海洋-气候系统的异步变化，并且可能代表了冰川消融期到全新世过渡期间海洋-大气重组的一个以前未被认识的组成部分。

ABSTRACT: The relationship between ocean circulation and monsoon systems over orbital to sub-millennial timescales is a crucial but poorly constrained component of the climate system. Here, using foraminiferal and detrital neodymium (Nd) isotope records from the intermediate-depth northern Indian Ocean, we provide new evidence revealing that both monsoon-driven weathering inputs and water mass advection from the Southern Ocean influenced past seawater Nd isotope changes in this region. Our results suggest that Indian Summer Monsoon weakening coincided with enhanced northward Antarctic Intermediate Water (AAIW) advection during the last deglaciation, reflecting a strong interhemispheric coupling. In contrast, the Early Holocene was characterized by enhanced monsoon strength but persistently strong AAIW inflow, indicating a relationship in the opposite sense. These differing interhemispheric relationships indicate asynchronous changes in the global atmosphere—ocean—climate system, and may represent a previously unrecognized

component of the ocean-atmosphere reorganization during the deglacial to Holocene transition.

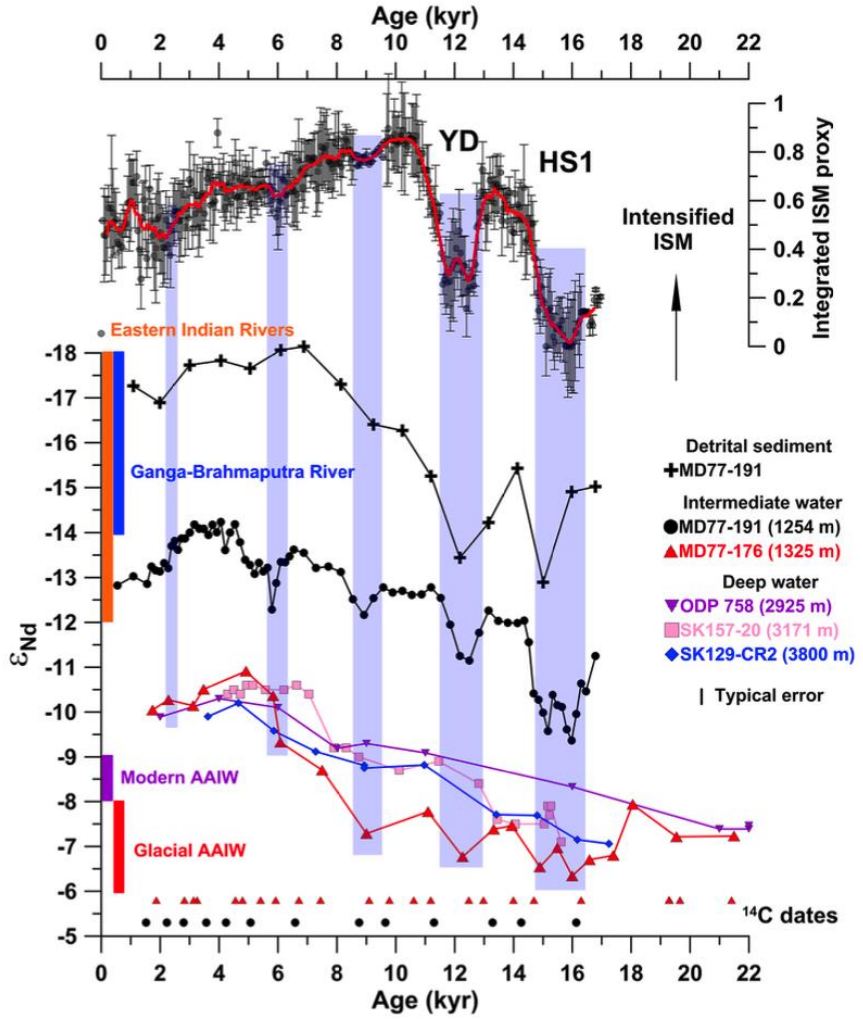

Figure 1. Comparison of foraminiferal and detrital Nd isotope records from core MD77-191 to existing seawater Nd isotope records from the northern Indian Ocean and the integrated Indian Summer Monsoon (ISM) proxy. Intermediate water Nd isotope records are from MD77-191 (this study) and MD77-176 (Yu et al., 2018). Deep water Nd isotope records are from ODP 758 (Burton & Vance, 2000), SK157-20 (Naik et al., 2019), and SK129-CR2 (Wilson, Piotrowski, et al., 2015). Blue bars indicate the consistent millennial-scale variations during HS1, the YD, and the Holocene. Colored bars along the Nd isotope axis indicate the end-members influencing core MD77-191: modern and glacial AAIW (purple and red; Amakawa et al., 2019; Hu et al., 2016; van de Flierdt et al., 2016), and weathering inputs from the Ganga-Brahmaputra River (blue) and eastern Indian rivers (orange; see Figure 1 for references). Typical error bar represents 2σ uncertainty for Nd

isotope analyses. The integrated ISM proxy record is plotted as gray circles, with a temporally varying error calculated using the double standard deviation of the overlapped intervals, while the red curve is a running mean with a window width of 9 (see Figures S4–S6 in Supporting Information S1 for details on the ISM proxy).

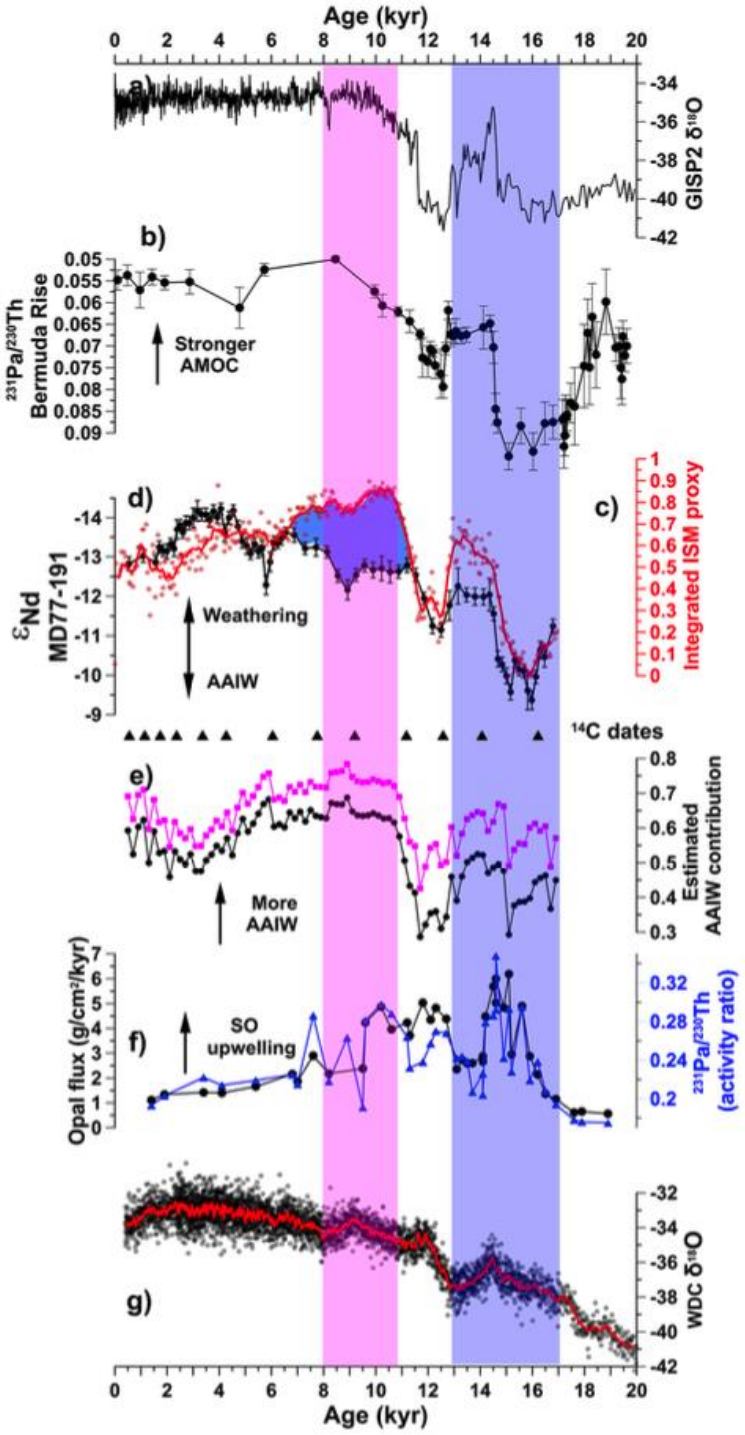

Figure 2. Chemical weathering and Antarctic Intermediate Water (AAIW) proxies in core MD77-

191 compared to Northern and Southern Hemisphere climate records. (a) Greenland ice core $\delta^{18}O$ record from GISP2 (Grootes & Stuiver, 1997). (b) Atlantic meridional overturning circulation (AMOC) intensity indicated by $^{231}Pa/^{230}Th$ excess at Bermuda Rise (McManus et al., 2004). (c) Integrated ISM proxy (this study; red line is a 9-point running mean; see Figures S4–S6 in Supporting Information S1 for details). (d) Nd isotope record from planktic foraminifera in core MD77-191 (this study). Radiocarbon dates in MD77-191 are shown with black triangles below this panel. (e) Estimated AAIW contribution calculated using Nd isotope records from ODP Site 1087 (magenta line) or core Y9 (black line) as the AAIW end-member (this study; see Figures S7–S8 in Supporting Information S1). Note that this sensitivity test indicates similar results for the two different AAIW end-member choices, with an absolute difference of about 10%. (f) Southern Ocean upwelling proxy records (Anderson et al., 2009). (g) Antarctic ice core $\delta^{18}O$ record (and 5-point running mean; red line) from WAIS Divide Core (WAIS Divide Project Members, 2013). Blue bar indicates the approximate timing of the deglaciation. Pink bar (and blue shaded area in panels (c–d)) indicates the Early Holocene decoupling between the ISM strength and the MD77-191 Nd isotope record, which is attributed to strengthened AAIW advection. Error bars in panels (b and d) are 2σ uncertainty.